DOI: 10.61782/fa.2025.0576

FORUM ACUSTICUM EURONOISE 2025

MODELING OF A SHIP SOUND RECORDED BY AN OCEAN BOTTOM SEISMOMETER

Samuel Pinson*

IRENAV EA 3624, École Navale, Lanvéoc, France

ABSTRACT

Cross-correlations of two hydrophone signals permit to deduce time-difference of arrivals (TDOA) and thus to locate sound sources. Trying to perform this signal processing techniques with hydrophones separated by great distances to locate ships present two problems. First the ship noise has a periodic nature from which correlations should also be -in principle- periodic (thus forbidding TDOA analysis). Second, the Doppler effect difference between the hydrophones may also prevent TDOAs to appear in correlations. In this communication, we present a ship noise model that generates similar signals to those recorded by an ocean bottom seismometer's hydrophone. This model considers that the ship sound is not perfectly periodic and includes water column reverberation through the image source method while the source is moving. The simulated signal quasi-periodic nature implies a finite support auto-correlation allowing TDOA analysis. It also reproduces time-frequency patterns very similar to those observed from an OBS hydrophone and thus is a good tool to explore signal processing techniques for sound source localization using greatly separated sensors.

Keywords: *ship noise modeling, ultra-low frequency, quasi-periodic signal, stochastic process, power-spectral density.*

**Corresponding author*: *samuel.pinson@ecole-navale.fr.*

1. INTRODUCTION

Use of ocean bottom seimometer (OBS) for ultra-low-frequency (ULF) passive-acoustic monitoring (PAM) has been of growing interest in recent years. Originally designed for geophysics studies, they are composed of a 3-axis accelerometer and an hydrophone with a sampling frequency around 100 Hz. Ref. [1] first reported blue whale and fin whale calls recorded by OBS's hydrophone. Then, the bioacoustics scientific communities expanded the possibility of using OBSs for PAM of baleen whales [2–6]. Recently, the underwater-acoustics (UWA) information from ship noise was used to accurately locate and orientate the OBSs [7] for geophysics purposes. On the contrary, further developments made use of OBSs for ship detection and tracking [8] over great distances of $\mathcal{O}(100\text{km})$. More recent work focused on OBS-signal decomposition into ship-traffic noise, baleen whale songs or seismic activity [9].

The context of this study is about OBS signal-processing designing to extract ship-noise time-difference of arrival (TDOA) between two OBSs. In multi-sensor signal processing, TDOAs are usually obtained through cross-correlations. In a first approximation, ULF ship noise can be considered as a periodic signal for which the cross-correlation is supposed to be also periodical with no clear TDOA. Nevertheless, under the hypothesis that ship-sound periodicity is not governed by an infinitely accurate atomic clock, one may assume that a cross-correlation should indeed present a maximum at the TDOA. The second problem for cross-correlations is the source relative velocity which might differ between OBSs due to their large separation (implying a different Doppler effect). Indeed, in frequency domain, the cross-correlation becomes

a spectral multiplication, and two narrow-band spectrum with a different Doppler shift gives a null result. Under those circumstances, a ship-noise model that accounts for the source quasi-periodicity, the water-column reverberation, and the Doppler effect, is presented in this paper.

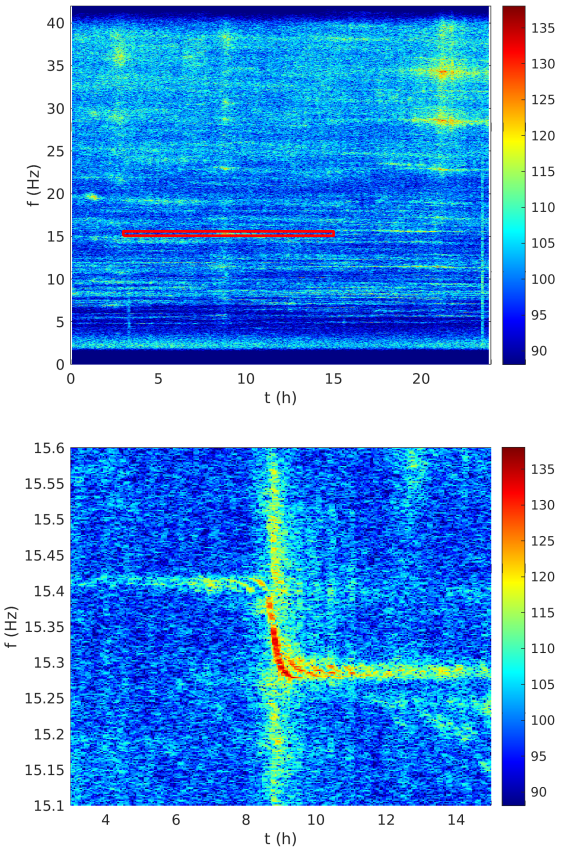

Figure 1. Top: 24h spectrogram from Nearest network OBS 22 (the 05/29/2007). Bottom: zoom on a ship harmonic. Colormap are in dB with arbitrary reference.

A closer look at an ULF ship noise is presented in Figure 1. Top figure shows a 24 h spectrogram (the 05/29/2007) from OBS 22 of the Nearest network [10] (OBS device description can be found in Ref. [11]). Sampling frequency was 100 Hz, the spectrogram time window is 10 mn (1.7 mHz frequency resolution) with 75% overlap. One can distinguish 3 ships passing by at 3h, 8h30 and 21h30. The red rectangle frames an harmonic of the second ship which the closest point of approach (CPA) was at 8h30, and its content is shown in bottom Figure 1. One can see the Doppler effect before and after the CPA and multiple S-shape curves at the CPA. The steepest CPA S shape corresponds to the direct path between the ship and the OBS, and other superposed S-shape curves get smoother as the number of reflections between the seafloor and the sea-surface increases.

The ship-noise model quasi-periodicity is described in section 2.1. Its time-domain water column reverberation by the image-source method (accounting for the Doppler effect) is presented in section 2.2. In section 3 a model simulation aims to replicate the spectrogram from Figure 1 (bottom). Section 4 concludes and discusses the implications of the ship-noise stochastic periodicity.

2. OBS SHIP RECORDS MODELING

2.1 Source signal

The quasi periodic signal with dominant frequency f_0 is modeled by quasi-periodic series of Dirac delta functions $\delta(t)$ convoluted with a minimum-phase pulse $e(t)$:

$$s(t) = e(t) * \sum_{k=-\infty}^{+\infty} \delta\left(t - kT_0 - \sum_{m=-\infty}^{k} \psi_m\right) , \quad (1)$$

where $T_0 = 1/f_0$, ψ_m is a zero-mean discrete Gaussian random fluctuation of the m^{th} period. The sum in the delta function argument means that the delay depends on all previous period fluctuations.

Changing the sum of random fluctuations into an integral of a continuous random fluctuation, eq. 1 becomes:

$$s(t) = \sum_{k=-\infty}^{+\infty} e\left(t - kT_0 - \int_{-\infty}^{t} \psi(u)\mathrm{d}u\right) . \quad (2)$$

where $\psi(u)$ is constant by steps for $kT_0 < t < (k+1)T_0$.

Making the change of variable $t' = t - \int^t \psi(u)\mathrm{d}u$ and using Poisson summation formula gives:

$$s(t) = \sum_{k=-\infty}^{+\infty} e\left(t' - kT_0\right) = \sum_{n=-\infty}^{+\infty} \tilde{e}(n\omega_0) \exp\left[\mathrm{i}n\omega_0 t'\right] , \quad (3)$$

where $\tilde{e}(\omega)$ is the Fourier transform of $e(t)$ and $\omega_0 = 2\pi/T_0$. Finally, the quasi-periodic source signal may be written by:

$$\begin{aligned} s(t) &= \sum_{n=-\infty}^{+\infty} s_n(t) \,, \\ &= \sum_{n=-\infty}^{+\infty} \tilde{e}(n\omega_0) \exp\left[\mathrm{i}n\omega_0 \left(t - \int^t \psi(u)\mathrm{d}u\right)\right] \,, \end{aligned} \tag{4}$$

where $s_n(t)$ is introduced to represent the n^{th} harmonic of the source signal.

Considering the n^{th} harmonic, the random variable $n\omega_0\psi(t)$ is the instant frequency fluctuation with a zero-mean Gaussian distribution, and $n\omega_0\phi(t) = n\omega_0 \int^t \psi(u)\mathrm{d}u$ is the phase fluctuation which is also Gaussian. The n^{th} harmonic auto-correlation function of the source signal is:

$$\begin{aligned} R_{ss}^n(\tau) &= E\left\{s_n(t)s_n^*(t-\tau)\right\} \,, \\ &= |\tilde{e}(n\omega_0)|^2 \exp\left[\mathrm{i}n\omega_0\tau\right] \\ &\quad \times E\left\{\exp\left[\mathrm{i}n\omega_0\left(\phi(t) - \phi(t-\tau)\right)\right]\right\} \,, \end{aligned} \tag{5}$$

where $E\{\,\cdot\,\}$ is the expected value. Recognizing the characteristic function of a Gaussian random variable in eq. 5, the auto-correlation becomes (Ref [12] p.162 table 5-2):

$$R_{ss}^n(\tau) = |\tilde{e}(n\omega_0)|^2 \exp\left[\mathrm{i}n\omega_0\tau - \frac{1}{2}n^2\omega_0^2\sigma_\phi^2(\tau)\right] \,, \tag{6}$$

where $\sigma_\phi^2(\tau)$ is the variance of $(\phi(t) - \phi(t-\tau))$. Assuming that random variables are ergodic, stationary and zero mean, the variance may be written (see Ref [12] p471 eq. 10.165):

$$\begin{aligned} \sigma_\phi^2(\tau) &= E\left\{\left(\phi(t) - \phi(t-\tau)\right)^2\right\} \,, \\ &= 2\int_0^\tau (\tau - \alpha) Cov_\psi(\alpha)\mathrm{d}\alpha \,. \end{aligned} \tag{7}$$

where $Cov_\psi(\alpha)$ is the covariance of the instant frequency fluctuation $\psi(t)$.

For the special case of uncorrelated period random fluctuations ($E\{\psi(t)^2\} = A^2$ and $E\{\psi(t)\psi(t+kT_0)\} = 0$ for $k \neq 0$), the instant-frequency fluctuation $\psi(u)$ is constant by step over each period and its covariance is:

$$\begin{aligned} Cov_\psi(\alpha) &= E\{\psi(u)\psi(u+\alpha)\} \,, \\ &= \lim_{T\to\infty} \frac{1}{T}\int_{-T/2}^{T/2} \psi(u)\psi(u+\alpha)\mathrm{d}u \,, \\ &= A^2\Lambda_{T_0}(\alpha) \,, \end{aligned} \tag{8}$$

where the triangle function $\Lambda_{T_0}(\alpha) = 1 - |\alpha|/T_0$ for $|\alpha| < T_0$ and 0 otherwise. Then the integral in eq. 7 gives:

$$\sigma_\phi^2(\tau) = A^2\tau^2\left(1 - \frac{2\,|\tau|}{3T_0}\right) \,, \tag{9}$$

for $|\tau| < T_0$, and for $|\tau| > T_0$ it gives:

$$\begin{aligned} \sigma_\phi^2(\tau) &= A^2 T_0\left(|\tau| - \frac{2T_0}{3}\right) \,, \\ &\approx A^2 T_0\,|\tau| \quad \text{for } |\tau| \gg T_0 \,. \end{aligned} \tag{10}$$

So neglecting the effect of the brief Gaussian shape at $|\tau| < T_0$, the autocorrelation of $s_n(t)$ has an exponential decay:

$$R_{ss}^n(\tau) \approx |\tilde{e}(n\omega_0)|^2 \exp\left[\mathrm{i}n\omega_0\tau - \tfrac{1}{2}(n\omega_0 A)^2 T_0\,|\tau|\right] \,, \tag{11}$$

for which the Fourier transform gives the power-law power-spectral density (PSD):

$$S_{ss}^n(\omega) \approx |\tilde{e}(n\omega_0)|^2 \frac{(n\omega_0 A)^2 T_0}{\left(\omega - n\omega_0\right)^2 + (n\omega_0 A)^4 T_0^2/4} \,, \tag{12}$$

One can note from PSD equations that the harmonics widen proportionally to n. A time domain signal is simulated using eq. 1 with a Dirac delta function for $e(t)$. The simulation parameters are: $f_0 = 10$, and $A = 5\%$ (meaning that the harmonic n instant frequency standard deviation is $0.05nf_0$). Figure 2 shows a comparison between its Welch periodogram (red curve) and a sum of eq. 12 over the harmonic number n (blue curve). One can see that the spectral shape shows well defined harmonics for low frequencies which slowly overlap as frequency increases, to finally merge into a flat spectrum.

2.2 Image source method for a moving source

The image-source method is used to model sound propagation from the source at $\mathbf{r}_s = (x_s, y_s, z_s)$ to the receiver

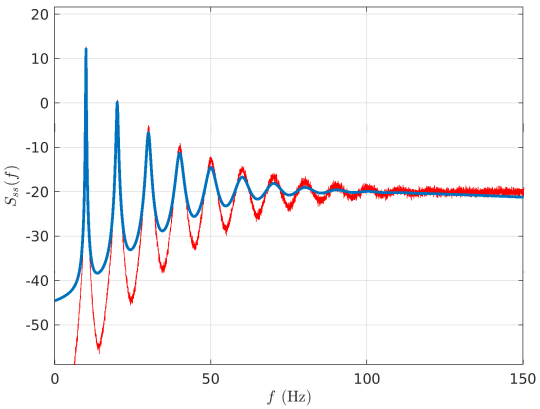

Figure 2. PSD of quasi-periodic Dirac delta functions (in dB). Red curve is the Welch periodogram of a simulated signal and the blue curve is eq. 11 summed over n.

at $\mathbf{r}_r = (x_r, y_r, z_r)$. Fig. 3 illustrates that wave-guide boundaries act as mirrors on which wave reflections may be interpreted as image sources. The source is moving along a line with a constant speed $\mathbf{v}$ and has a directivity pattern $\mathcal{D}(\theta, \chi)$ where θ is the horizontal angle relative to its direction and χ is the elevation angle (corresponding to the grazing angle in the propagation plane). So most parameters (except receiver position) depend on time.

In a constant depth H and isovelocity water column, the field from a moving point source can be modeled by image sources:

$$p(\mathbf{r}_r, t) = \sum_{q=0,1} \sum_{n=-\infty}^{+\infty} \mathcal{D}(\theta, \chi_n) V_B^{|n+q|}(\chi_n) V_T^{|n|}(\chi_n) \times \frac{s(t - d_n/c)}{d_n}, \tag{13}$$

where $s(t)$ the emitted signal, χ_n the grazing angles, c the water sound speed, $V_B(\chi_n)$ and $V_T(\chi_n)$ are the reflection coefficients from the bottom and the top of the water column, and:

$$\begin{aligned} d_n &= \left(r^2 + (z_r - (-1)^q z_s + 2Hn)^2\right)^{1/2}, \\ \chi_n &= \tan^{-1} \frac{|z_r - (-1)^q z_s + 2Hn|}{r}, \\ r &= \left((x_r - x_s)^2 + (y_s - y_r)^2\right)^{1/2}. \end{aligned} \tag{14}$$

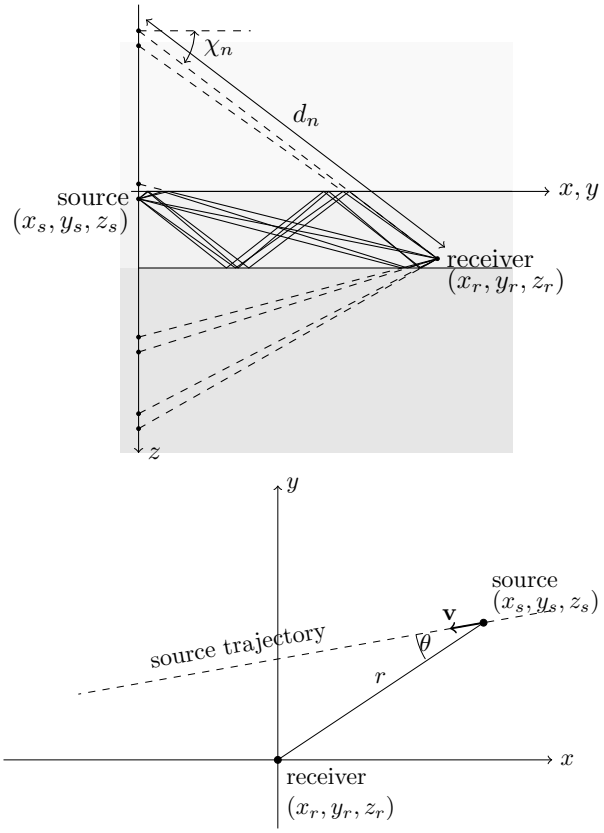

Figure 3. Top: wave-guide interface reflections interpreted as image sources in the propagation plane. Bottom: Geometry in the horizontal plane.

Note that the Doppler effect is included in eq. 13 through the time dependence of source coordinates.

3. MODELING EXAMPLE

For the modeling example, the cargo-ship harmonic at 15.35 Hz in Figure 1 is replicated. From the S shape in the spectrogram, it is easy to deduce from the Doppler shifts that the cargo speed is 6 m/s. Thus the 12 hours spectrogram span corresponds to a 260 km ship travel. Knowing the OBS is 4095 m deep, the ship horizontal distance relative to the OBS at the CPA can be found by fitting a theoretical Doppler S-shape curve into the spectrogram. Doing so, it is found that the ship passes right above the OBS. Finally, the periodicity randomness A is adjusted by trial and error to match the observed harmonic thickness at $A = 1.5\%$. Source depth is set to 7 m and the OBS

height above the seafloor is set to 30 cm. Seafloor reflection coefficient is calculated with a seabed density of 2 and a 1800 m/s sound-speed. The ship directivity is set higher at its rear with $\mathcal{D}(\theta, \chi_n) = (2 - \cos\theta)/3$. Finally, 24 rays are used to model the water column reverberation. They correspond to 6 group of 4 rays with close arrival time (2 groups of 4 rays with close arrival time are illustrated in Figure 3). The first group of 4 rays may be considered as the direct path, the second as the seaFloor-seaSurface-seaFloor (FSF) path, the third as the FSFSF path, *etc*. The result of the simulation is shown in Figure 4 and it compares well with The spectrogram in Figure 1. 2 distinguishable S curves corresponding to the direct and FSF paths indicate echoes with different Doppler effects near the CPA. More S curves could be distinguishable with a lower periodicity randomness.

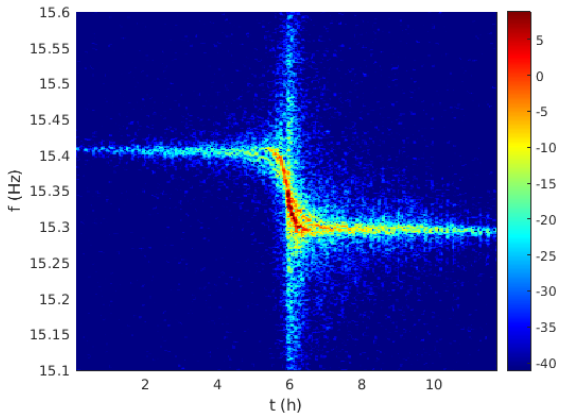

Figure 4. Spectrogram of a simulated data made to mimic the spectrogram in Figure 1. Colormap is in dB with arbitrary reference.

4. DISCUSSION

The ship-noise model presented in this paper is realistic enough to compare well with observed data. So it can be a useful tool to design signal-processing techniques on ULF OBS signals. Accounting for the stochastic nature of ship-noise periodicity permits to replicate their harmonic thicknesses observed from real data spectrograms. Moreover, the time-domain image-source method replicates the spectrogram Doppler patterns. However the application extents of the model are limited by the simplistic representation of the acoustic waveguide. Neither the sound-speed profile, the topography or the seafloor complexities are accounted for.

In ULF cargo ship noise research area, propeller sheet cavitation is known to be the main contributor to the radiated sound. This sound is mostly harmonic but tend to present a broadband noise appearing roughly above 50 Hz [13, 14]. As seen in Figure 2, the possibility that the stochastic nature of signal periodicity might shed some light on this broadband noise is worth to be investigated in future work.

5. ACKNOWLEDGMENTS

This work was partially funded by the ANR Astrid RESSACH under grant number ANR-22-ASTR-0030. The author thanks Mechita Schmidt-Aursch for providing information about the Nearest seismic network, and greatly acknowledges Richard Dréo who shared his findings on the cargo ship harmonic patterns and for his enlightening discussions about ULF acoustics using OBS.

6. REFERENCES

[1] M. A. McDonald, J. A. Hildebrand, and S. C. Webb, "Blue and fin whales observed on a seafloor array in the northeast pacific," *The Journal of the Acoustical Society of America*, vol. 98, no. 2, pp. 712–721, 1995.

[2] R. A. Dunn and O. Hernandez, "Tracking blue whales in the eastern tropical pacific with an ocean-bottom seismometer and hydrophone array," *The Journal of the Acoustical Society of America*, vol. 126, no. 3, pp. 1084–1094, 2009.

[3] D. Harris, L. Matias, L. Thomas, J. Harwood, and W. H. Geissler, "Applying distance sampling to fin whale calls recorded by single seismic instruments in the northeast atlantic," *The Journal of the Acoustical Society of America*, vol. 134, no. 5, pp. 3522–3535, 2013.

[4] R. Dreo, L. Bouffaut, L. Guillon, V. Labat, G. Barruol, and A.-O. Boudraa, "Antartic blue whale localization with ocean bottom seismometers in southern indian ocean," *UACE2017 - 4th Underwater Acoustics Conference and Exhibition, Greece*, 2017.

[5] R. Dréo, L. Bouffaut, E. Leroy, G. Barruol, and F. Samaran, "Baleen whale distribution and seasonal occurrence revealed by an ocean bottom seismometer network in the western indian ocean," *Deep Sea*

Research Part II: Topical Studies in Oceanography, vol. 161, pp. 132–144, 2019.

[6] L. Bouffaut, *Détection et classification dans un contexte acoustique passive: application à la détection des signaux basse-fréquences des baleines bleues*. PhD thesis, Université de Bretagne occidentale-Brest, 2019.

[7] A. Trabattoni, G. Barruol, R. Dreo, A. Boudraa, and F. Fontaine, "Orienting and locating ocean-bottom seismometers from ship noise analysis," *Geophysical Journal International*, vol. 220, no. 3, pp. 1774–1790, 2020.

[8] A. Trabattoni, G. Barruol, R. Dréo, and A. Boudraa, "Ship detection and tracking from single ocean-bottom seismic and hydroacoustic stations," *The Journal of the Acoustical Society of America*, vol. 153, no. 1, pp. 260–273, 2023.

[9] J. Lecoulant, A.-O. Boudraa, and S. Pinson, "Non-negative matrix factorization based single-channel source-separation of passive underwater acoustic signals in deep sea," *JASA Express Letters*, vol. 5, no. 2, p. 026004, 2025.

[10] W. Geissler, L. Matias, D. Stich, F. Carrilho, W. Jokat, S. Monna, A. IbenBrahim, F. Mancilla, M.-A. Gutscher, V. Sallarès, *et al.*, "Focal mechanisms for sub-crustal earthquakes in the gulf of cadiz from a dense obs deployment," *Geophysical Research Letters*, vol. 37, no. 18, 2010.

[11] M. Schmidt-Aursch and C. Haberland, "Depas (deutscher geräte-pool für amphibische seismologie): German instrument pool for amphibian seismology," *Journal of large-scale research facilities*, vol. 3, no. A122, 2017.

[12] A. Papoulis and S. U. Pillai, *Probability, random variables, and stochastic processes, Fourth Edition*. McGraw-Hill Europe: New York, NY, USA, 2002.

[13] G. Tani, M. Viviani, J. Hallander, T. Johansson, and E. Rizzuto, "Propeller underwater radiated noise: A comparison between model scale measurements in two different facilities and full scale measurements," *Applied Ocean Research*, vol. 56, pp. 48–66, 2016.

[14] L. S. Föhring, P. M. Juhl, and D. Wittekind, "On the influence of cavitation volume variations on propeller broadband noise," *Journal of Marine Science and Engineering*, vol. 10, no. 12, p. 1946, 2022.